

# Supporting Information

Soppina et al. 10.1073/pnas.1400759111

## SI Materials and Methods

**Plasmids and Antibodies.** Plasmids for mammalian expression of KIF1A and KIF13A (1, 2) were a gift of Gary Banker (Oregon Health Sciences University, Portland, OR), and plasmids for expression of KIF13B (3) and KIF16B (4) were gifts of Hiroaki Miki (Department of Cellular Regulation, Research Institute for Microbial Diseases, Osaka University, Osaka, Japan) and Marino Zerial (Max Planck Institute of Molecular Cell Biology and Genetics, Dresden, Germany), respectively. Fluorescently tagged versions of full-length or truncated motors were generated using appropriate restriction sites or PCR amplification and subcloned into mCitrine-N1/C1 and/or 3xmCitrine-N1/C1 vectors (based on Clontech's EYFP-N1/C1 vectors). Mutations were generated by QuikChange site-directed mutagenesis (Stratagene) or by overlapping PCR. For Förster resonance energy transfer (FRET) assays, full-length KIF16B wild-type and the cargo-binding LF/AA mutant (L1248A and F1249A) were cloned into both donor (mCFP-N1/C1) and acceptor (mCit-N1/C1) vectors. For the neck coil (NC) mutant, the hydrophobic residues in the "a" and "d" positions of the NC (Fig. 2C) were changed to glutamate and lysine residues respectively, as described for *CeUNC-104* (5). For FP-PX, the monomeric KIF16B-PX domain (aa1182–1317) was cloned into donor (mCFP-C1) or acceptor (mCit-C1) vector. For FP-SAH-PX, a 30-nm single  $\alpha$ -helix (SAH) from the *Trichomonas vaginalis* G3 Kelch family protein (6) was cloned between the FP and PX domain in the FP-PX construct. All plasmids were verified by DNA sequencing. The constitutively motile dimeric kinesin-1 construct KHC(1–560)-3xmCitrine has been described (7). The following antibodies were used: GFP (A6455; Invitrogen), EEA1 (610457; BD Biosciences),  $\beta$ -tubulin (E7; Developmental Studies Hybridoma Bank, University of Iowa).

**Cell Culture and Transfection.** COS-7 (monkey kidney fibroblast, ATCC) cells were grown in DMEM + 10% (vol/vol) FBS and 2 mM L-glutamine at 37 °C with 5% (vol/vol) CO<sub>2</sub>. Cells were transfected with 1.0  $\mu$ g of plasmid DNA using Expressfect (Danville Scientific). The next day, cells were lysed or processed for microscopy. The mouse catecholaminergic cell line CAD (8) was grown in a 1:1 mixture of F12:DMEM (BioWhittaker) plus 10% (vol/vol) FBS (HyClone) at 37 °C with 5% (vol/vol) CO<sub>2</sub>. Cells were induced to differentiate by transfer to serum-free media and then transfected with 1.0  $\mu$ g of plasmid DNA using TransIT-LT1 (Mirus-Bio). After 2 d, the cells were processed for fluorescence microscopy.

**Immunostaining and Fluorescence Microscopy.** Cells were rinsed with PBS, fixed in 4% (vol/vol) paraformaldehyde in PBS for 10 min, quenched with 50 mM ammonium chloride in PBS for 5 min, permeabilized in 0.2% Triton X-100 in PBS for 5 min, and blocked with 0.2% fish skin gelatin (FSG) in PBS for 5 min. Primary and secondary antibody incubations were carried out in PBS/FSG for 1 h each and the coverslips were mounted in Prolong Gold (Life Technologies). Images were obtained on an inverted epifluorescence microscope Nikon TE2000E, equipped with 60 $\times$  1.40 N.A. objective and a Photometrics CoolSnap HQ camera.

**CAD Cell Assay.** To rapidly screen motors for processive motility, mCit-tagged versions were expressed in differentiated neuronal CAD cells where the spatial segregation of microtubule minus ends in the cell body and plus ends in neurite tips enables the charac-

teristic accumulation of processive kinesin motors in the neurite tips (1, 2, 9–12). To quantify motor distribution, we manually measured the average fluorescence intensity of the cell body and its neurite tip using ImageJ software. The data are reported as the ratio of average fluorescence intensity in the neurite tip to that in the cell body. The mean and SD for each motor were plotted in graphs using Prism 6 software (GraphPad).

**COS-7 Cell Lysates.** COS-7 cells expressing fluorescent protein FP-tagged motors were trypsinized and harvested by low-speed centrifugation at 4 °C. The pellet was washed once with DMEM and lysed in ice-cold lysis buffer (25 mM Hepes/KOH, 115 mM potassium acetate, 5 mM sodium acetate, 5 mM MgCl<sub>2</sub>, 0.5 mM EGTA, and 1% Triton X-100, pH 7.4) freshly supplemented with 1 mM PMSF and protease inhibitors (10  $\mu$ g/mL leupeptin, 5  $\mu$ g/mL chymostatin, 3  $\mu$ g/mL elastatinal, and 1 mg/mL pepstatin). The lysate was clarified by centrifugation at 16,000  $\times$  g at 4 °C and either used fresh for assays or aliquots were frozen in liquid nitrogen and stored at –80 °C until further use.

**Single-Molecule Assays by Total Internal Reflection Fluorescence Microscopy.** All single-molecule assays were performed using a Nikon Ti-E objective-type total internal reflection fluorescence (TIRF) microscope with Perfect Focus System, a 100 $\times$  1.49 N.A. CFI APO TIRF objective, an Agilent 3-Line (488, 561, and 640 nm) Monolithic Standard Power Laser Launch with AOTF, an EMCCD camera (iXon<sup>+</sup> DU897; Andor), and controlled by Nikon Elements image acquisition software.

All assays were performed at room temperature in a narrow flow-cell (~10  $\mu$ L volume) prepared by attaching a clean number 1.5 coverslip to a microscope slide with double-sided adhesive tape. Microtubules were polymerized from purified tubulin (TL238, Cytoskeleton) in BRB80 buffer (80 mM Pipes/KOH, pH 6.8, 1 mM MgCl<sub>2</sub>, and 1 mM EGTA) supplemented with 1 mM GTP at 37 °C for 20 min. Polymerized microtubules were stored at room temperature after addition of five volumes of prewarmed BRB80 containing 20  $\mu$ M taxol and additional 5 min incubation at 37 °C. Polymerized microtubules were diluted in P12 buffer (12 mM Pipes/KOH, pH 6.8, 1 mM MgCl<sub>2</sub>, and 1 mM EGTA) freshly supplemented with 10  $\mu$ M taxol and then infused into a flow-cell and incubated for 5 min at room temperature to adsorb onto the coverslip. Subsequently, 50  $\mu$ L of blocking buffer (10 mg/mL BSA in P12 buffer with 10  $\mu$ M taxol) was introduced and incubated for 20 min to prevent nonspecific binding of kinesin motors onto the coverslip surface. Finally, kinesin motors in a 50- $\mu$ L Motility Mix (0.1–2.0  $\mu$ L of COS-7 cell lysate with 30  $\mu$ L of blocking buffer, 15  $\mu$ L of P12 buffer, 2 mM nucleotide, 0.5  $\mu$ L of 100 mM DTT, 0.5  $\mu$ L of 100 mM MgCl<sub>2</sub>, and 0.5  $\mu$ L each of 20 mg/mL glucose oxidase, 8 mg/mL catalase, and 1 M glucose) was added to the flow chamber and the ends were sealed with molten paraffin wax. For motility assays under high-ionic-strength buffers, the P12 buffer in motility mix was replaced with cellular buffer (25 mM Hepes/KOH, 115 mM potassium acetate, 5 mM sodium acetate, 5 mM MgCl<sub>2</sub>, and 0.5 mM EGTA, pH 7.4) or BRB80 (80 mM Pipes/KOH, pH 6.8, 1 mM MgCl<sub>2</sub>, and 1 mM EGTA).

**Motility assays.** 3xmCit-tagged motors in Motility Mix with 2 mM ATP were imaged at 20 frames per second without binning and at low laser power to avoid photobleaching during processive motor runs. The position of fluorescent motor spots was manually tracked frame-by-frame using a custom-written plugin in ImageJ

(National Institutes of Health) as described (13). The velocities and run lengths of individual motors were binned and histograms were generated for the population by plotting the number of events in each bin. The average velocity and run length were then obtained by fitting a single Gaussian peak to the population histogram. These run lengths are likely to be an underestimate because many motors reached the end of the microtubule track before ending their run. The measurements for each construct come from at least two independent protein preparations and include motile events lasting at least 10 frames (500 ms) except for wild-type full-length kinesin-3 motors, where a minimum of five frames (250 ms) was used. All data are presented as mean  $\pm$  SE of mean (SEM). All *P* values were calculated by using a two-tailed unpaired Student *t* test.

**Photobleaching assays.** 3xmCit-tagged motors were either attached to microtubules in the presence of 2 mM adenylylimidodiphosphate (AMPPNP) or adsorbed to the coverslip. Subsequently, the flow chamber was washed once with Motility Mix lacking COS-7 lysate to remove unbound motors and then imaged at 20 frames per second. The intensity profile of individual fluorescent spots was tracked frame-by-frame using custom-written plugins in ImageJ (National Institutes of Health). The number of bleaching steps was determined for each spot and then plotted in a histogram to show the population distribution. As photobleaching of each FP is a discrete process, the fluorescence intensity of a protein complex with multiple FPs bleaches in a step-like manner indicative of the number of FPs in the complex (14). For 3xmCit-tagged motors, dimeric motors [e.g., KHC(1–560)] contain six FPs and the majority of molecules bleach in four to six steps, whereas monomeric motors [e.g., KIF1A(1–381)] contain three FPs and the majority of molecules bleach in two or three steps (13, 15).

**Diffusion assays.** 3xmCit-tagged motors in Motility Mix with 2 mM ATP or ADP were imaged at 60 frames per second and the motility of individual spots was analyzed using a custom-written MATLAB program based on ref. 16. A Gaussian mixture model was implemented for detecting individual particles and gap closing and motion propagation features were implemented for tracking the detected particles frame-by-frame. Microtubule-based events were selected based on their asymmetric positioning over subsequent frames (a trajectory with preferred directionality), whereas non-microtubule-based events were eliminated based on their symmetric positioning over subsequent frames (symmetric scattering of a Brownian trajectory) (17). Finally, we considered only events which lasted more than 10 frames to calculate the MSD using the following equation:

$$MSD = \langle L^2(\Delta t) \rangle = \frac{1}{N-n} \sum_{j=1}^2 \sum_{k=1}^{N-n} [x_j((k+n)\delta t) - x_j(k\delta t)]^2$$

$$\Delta t = n\delta t$$

$$1 \leq n \leq N-1,$$

where  $\delta t$  is the time interval between frames and *N* is the total frame number. For curve fitting, we used the third to seventh data points and applied the standard least-squares method.

**Landing assays.** For each construct, equal amounts of motor lysate was added to flow-cells in different ionic strength buffers and imaged at 20 frames per second. The number of motors landing on a microtubule was counted and then divided by the total length of the microtubules and the recording time to obtain a landing rate with the units of events/ $\mu$ m/min.

**Live-Cell FRET Microscopy.** Live-cell FRET measurements were made in COS-7 cells expressing fluorescently tagged donor (mCFP) and acceptor (mCit) proteins as described (18, 19). All imaging was performed in a wide-field Olympus (IX70) inverted microscope calibrated to obtain the parameters  $\alpha$ ,  $\beta$ ,  $\gamma$ , and  $\xi$  from COS-7 cells expressing mCit ( $\alpha$ ), mCFP ( $\beta$ ), or a mCFP-mCit molecule linked by 16 aa ( $\gamma$  and  $\xi$ ) whose FRET efficiency (*E*) was measured by fluorescence lifetime spectroscopy (18). Images were obtained with a 40 $\times$  (LCPLanFl, N.A. 0.6) objective, 1.5 $\times$  tube lens, and excitation nm(BP)/emission nm(BP) filters for imaging mECFP donor fluorescence ( $I_D$ ): 436(10)/465 (30), mCit acceptor fluorescence ( $I_A$ ): 492(18)/535(30), or FRET ( $I_F$ ): 436(10)/535(30). The three fluorescence images ( $I_D$ ,  $I_A$ , and  $I_F$ ) were corrected for illumination shading and bias offset and then used to calculate three parameters that describe each pixel: (i)  $R_M$ , the mole ratio of acceptor- to donor-labeled proteins, (ii)  $E_A$ , the apparent acceptor FRET efficiency (FRET efficiency  $\times$  fraction of acceptor molecules in complex), and (iii)  $E_D$ , the apparent donor FRET efficiency (FRET efficiency  $\times$  fraction of donor molecules in complex).  $E_A$  and  $E_D$  range between 0 and 100%, where 100% indicates all acceptor and donor molecules in the FRET complex and with complete energy transfer. Because protein expression levels influence the fraction of donor or acceptor molecules in FRET complex, we analyzed cells with  $R_M$  close to 1.0 and we calculated an average FRET efficiency,  $E_{AVE} = (E_D + E_A)/2$ , which is less sensitive to expression ratio (19). At least 25 cells were imaged for each construct. A two-tailed *t* test was used to compare steady-state  $E_{AVE}$  values across constructs.

- Jacobson C, Schnapp B, Banker GA (2006) A change in the selective translocation of the kinesin-1 motor domain marks the initial specification of the axon. *Neuron* 49(6):797–804.
- Huang CF, Banker G (2012) The translocation selectivity of the kinesins that mediate neuronal organelle transport. *Traffic* 13(4):549–564.
- Yoshimura Y, Terabayashi T, Miki H (2010) Par1b/MARK2 phosphorylates kinesin-like motor protein GAKIN/KIF13B to regulate axon formation. *Mol Cell Biol* 30(9):2206–2219.
- Hoepfner S, et al. (2005) Modulation of receptor recycling and degradation by the endosomal kinesin KIF16B. *Cell* 121(3):437–450.
- Klopfenstein DR, Tomishige M, Stuurman N, Vale RD (2002) Role of phosphatidylinositol (4,5)bisphosphate organization in membrane transport by the Unc104 kinesin motor. *Cell* 109(3):347–358.
- Sivaramakrishnan S, et al. (2009) Combining single-molecule optical trapping and small-angle x-ray scattering measurements to compute the persistence length of a protein ERK alpha-helix. *Biophys J* 97(11):2993–2999.
- Friedman DS, Vale RD (1999) Single-molecule analysis of kinesin motility reveals regulation by the cargo-binding tail domain. *Nat Cell Biol* 1(5):293–297.
- Qi Y, Wang JK, McMillian M, Chikarishi DM (1997) Characterization of a CNS cell line, CAD, in which morphological differentiation is initiated by serum deprivation. *J Neurosci* 17(4):1217–1225.
- Nakata T, Hirokawa N (2003) Microtubules provide directional cues for polarized axonal transport through interaction with kinesin motor head. *J Cell Biol* 162(6):1045–1055.
- Lee JR, et al. (2004) An intramolecular interaction between the FHA domain and a coiled coil negatively regulates the kinesin motor KIF1A. *EMBO J* 23(7):1506–1515.
- Hammond JW, Blasius TL, Soppina V, Cai D, Verhey KJ (2010) Autoinhibition of the kinesin-2 motor KIF17 via dual intramolecular mechanisms. *J Cell Biol* 189(6):1013–1025.
- Huo L, et al. (2012) The CC1-FHA tandem as a central hub for controlling the dimerization and activation of kinesin-3 KIF1A. *Structure* 20(9):1550–1561.
- Cai D, Verhey KJ, Meyhöfer E (2007) Tracking single Kinesin molecules in the cytoplasm of mammalian cells. *Biophys J* 92(12):4137–4144.
- Ulbrich MH, Isacoff EY (2007) Subunit counting in membrane-bound proteins. *Nat Methods* 4(4):319–321.
- Hammond JW, et al. (2009) Mammalian kinesin-3 motors are dimeric in vivo and move by processive motility upon release of autoinhibition. *PLoS Biol* 7(3):e72.
- Jaqaman K, et al. (2008) Robust single-particle tracking in live-cell time-lapse sequences. *Nat Methods* 5(8):695–702.
- Huet S, et al. (2006) Analysis of transient behavior in complex trajectories: Application to secretory vesicle dynamics. *Biophys J* 91(9):3542–3559.
- Hoppe A, Christensen K, Swanson JA (2002) Fluorescence resonance energy transfer-based stoichiometry in living cells. *Biophys J* 83(6):3652–3664.
- Cai D, Hoppe AD, Swanson JA, Verhey KJ (2007) Kinesin-1 structural organization and conformational changes revealed by FRET stoichiometry in live cells. *J Cell Biol* 176(1):51–63.







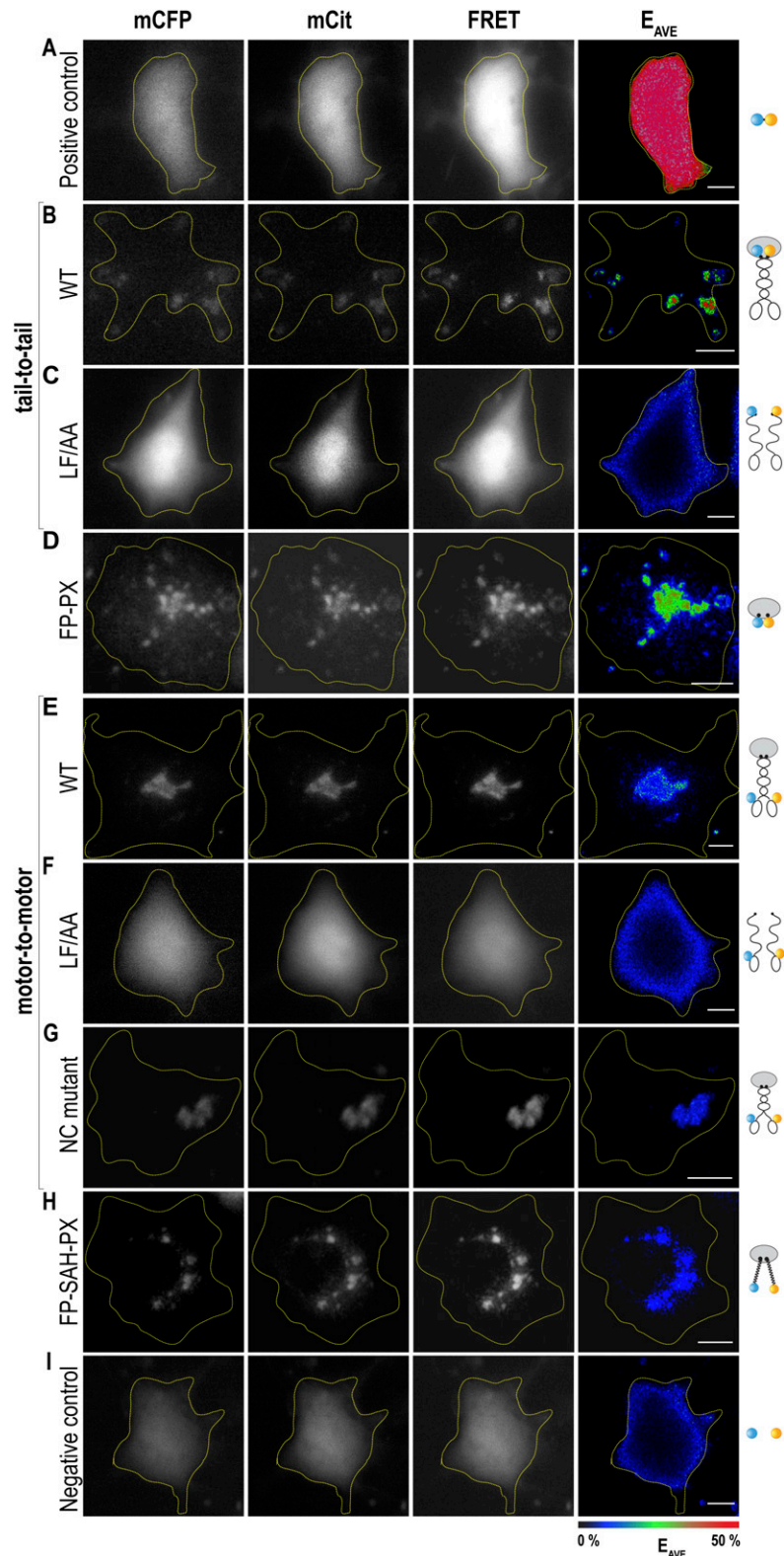


**Fig. S3.** FRET microscopy in live COS-7 cells. Shown are representative images taken under mCFP imaging (first column), mCit imaging (second column), or FRET imaging (third column) conditions. From these images, the average FRET efficiency ( $E_{AVE}$ ) (fourth column) was calculated. (A) As a positive FRET control, a mCFP-mCit fusion protein (linked by 16 aa) was expressed. High levels of FRET were observed (maximum FRET signal). (B and E) Wild-type or (C and F) LF/AA mutant KIF16B motors were tagged with mCFP or mCit at (B and C) their C termini to measure FRET between the tail domains of individual KIF16B motors or at (E and F) their N termini to measure FRET between the motor domains of individual KIF16B motors. (D) FP-PX, the monomeric KIF16B-PX domain, was fused with mCFP or mCit. (B and E) Coexpression of mCFP- and mCit-tagged wild-type motors reveals a high FRET signal on the endosomal cargo, indicating that cargo-bound motors are dimeric in nature. That FRET pairs on the C terminus of KIF16B (B) give a higher FRET signal than FRET pairs on the N terminus of KIF16B (E) indicates that the tail domains are in closer proximity to each other than are the motor domains when KIF16B is in a dimeric state. (C and F) Legend continued on following page

Coexpression of mCFP- and mCit-tagged LF/AA motors reveals little to no FRET signal, indicating that non-cargo-bound motors are monomeric in nature. (G) NC mutant, the hydrophobic residues in the "a" and "d" positions of the KIF16B neck coil (Fig. 2C), were changed to glutamate and lysine residues, respectively. (H) FP-SAH-PX, a 30-nm single  $\alpha$ -helix (SAH) from the *Trichomonas vaginalis* G3 Kelch family protein was inserted between the FP and PX domain in the FP-PX construct. (I) As a negative FRET control, the FRET donor mECFP and FRET acceptor mCit proteins were coexpressed. Little to no FRET was observed (background FRET signal). (Scale bars, 10  $\mu$ m.)

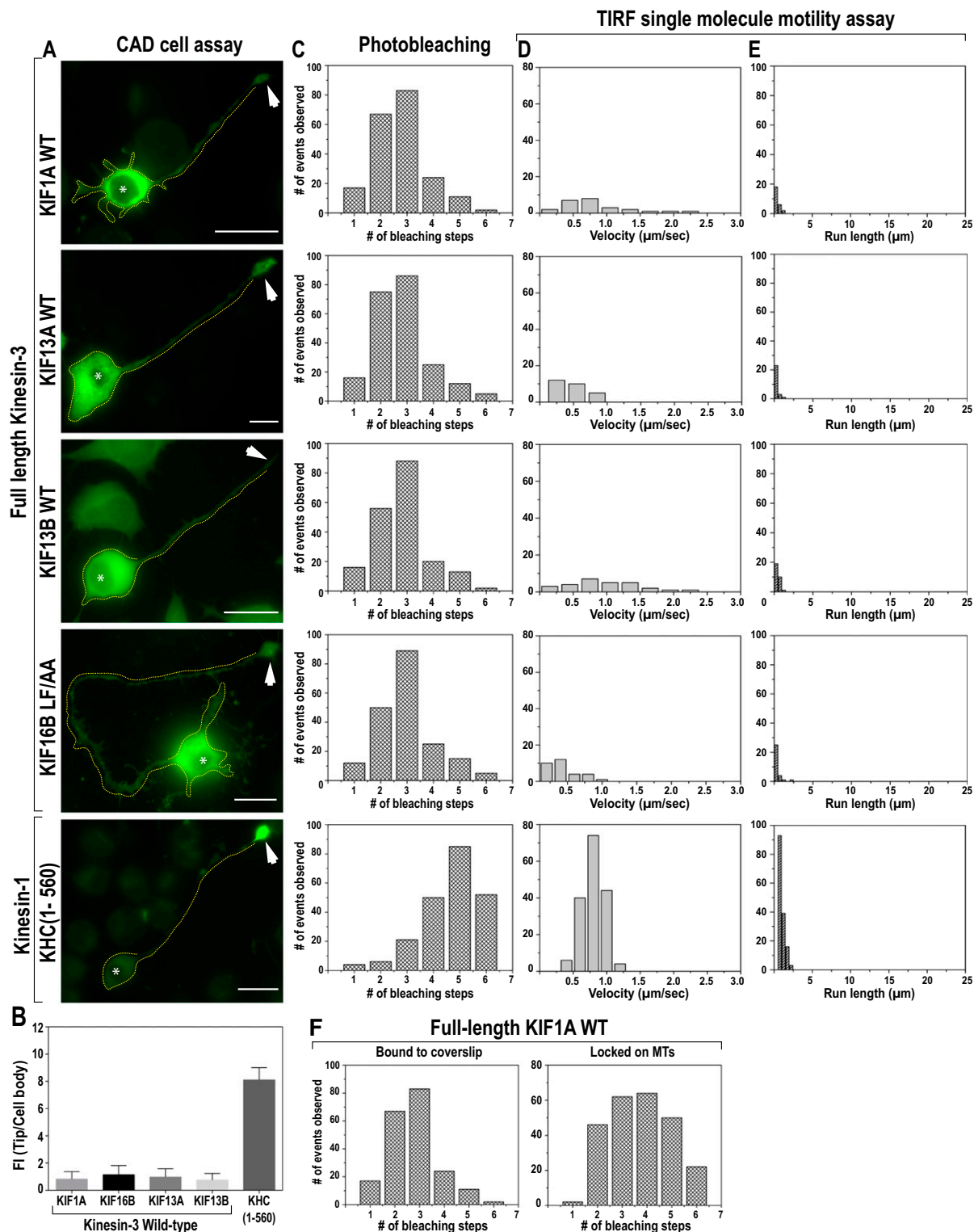


**Fig. S4.** Full-length kinesin-3 motors are largely monomeric and are inactive. The oligomeric state and motility properties of wild-type full-length kinesin-3 motors KIF1A, KIF16B(LF/AA), KIF13A, and KIF13B were compared with that of an active dimeric kinesin-1 [KHC(1–560)] motor. (A) CAD cell assay to measure motor processivity. Representative images of differentiated CAD cells expressing wild-type full-length kinesin-3 motors or KHC(1–560) (all with C-terminal mCit tag). Processive motors move to the plus ends of microtubules and thus accumulate at the tips of neurites, whereas inactive motors remain in the cell body (1–6). The full-length kinesin-3 motors localized to the cell bodies, indicative of nonprocessive motors, whereas KHC(1–560) accumulated in neurite tips, indicative of a processive motor. Expressing cells are outlined with a yellow dotted line. Arrowheads indicate neurite tips. White asterisks indicate nuclei. (Scale bars, 20  $\mu\text{m}$ .) (B) Quantification of the CAD cell tip accumulation is presented as the ratio of the average fluorescence intensity (FI) in the neurite tip to that in the cell body.  $n = 15\text{--}20$  cells each. The values and error bars represent mean  $\pm$  SD. (C) Photobleaching assay to measure oligomeric state. The fluorescence intensity over time was measured by TIRF microscopy for individual 3xCit-tagged motors in COS-7 cell lysates directly adsorbed onto the coverslip. The number of bleaching events per molecule was plotted in a histogram for the population. The majority of full-length kinesin-3 motors bleached in one to three steps, indicating that

Legend continued on following page

most of the molecules in the population are in a monomeric state. The majority of KHC(1–560) motors bleached in four to six steps, indicative of dimeric motors. (*D* and *E*) Single-molecule motility assays. 3xmCit-tagged motors in COS-7 cell lysates were added to polymerized microtubules in a flow chamber and observed by TIRF microscopy. The measured velocities (*D*) and run lengths (*E*) of each population were plotted in a histogram. Very few motility events were observed for the full-length kinesin-3 motors, indicating that these motors are inactive, and the few observed motility events were short-lived. Robust motility was observed for dimeric KHC(1–560)-3xmCit. (*F*) The finding that full-length KIF1A is monomeric differs from our previous published work (6), where expressed full-length motors were found to be in a predominantly dimeric state. However, the previous photobleaching assays were carried out in the presence of microtubules and AMPPNP and therefore enriched for the subpopulation of dimeric motors, which have a higher microtubule affinity than monomeric motors (7). Direct comparison of the photobleaching behavior of full-length KIF1A motors in the soluble (adsorbed to the coverslip) versus microtubule-bound state demonstrates that soluble motors are largely monomeric.

- Jacobson C, Schnapp B, Banker GA (2006) A change in the selective translocation of the Kinesin-1 motor domain marks the initial specification of the axon. *Neuron* 49(6):797–804.
- Huang CF, Banker G (2012) The translocation selectivity of the kinesins that mediate neuronal organelle transport. *Traffic* 13(4):549–564.
- Nakata T, Hirokawa N (2003) Microtubules provide directional cues for polarized axonal transport through interaction with kinesin motor head. *J Cell Biol* 162(6):1045–1055.
- Lee JR, et al. (2004) An intramolecular interaction between the FHA domain and a coiled coil negatively regulates the kinesin motor KIF1A. *EMBO J* 23(7):1506–1515.
- Huo L, et al. (2012) The CC1-FHA tandem as a central hub for controlling the dimerization and activation of kinesin-3 KIF1A. *Structure* 20(9):1550–1561.
- Hammond JW, et al. (2009) Mammalian kinesin-3 motors are dimeric in vivo and move by processive motility upon release of autoinhibition. *PLoS Biol* 7(3):e72.
- Rashid DJ, Bononi J, Triplet BP, Hodges RS, Pierce DW (2005) Monomeric and dimeric states exhibited by the kinesin-related motor protein KIF1A. *J Pept Res* 65(6):538–549.

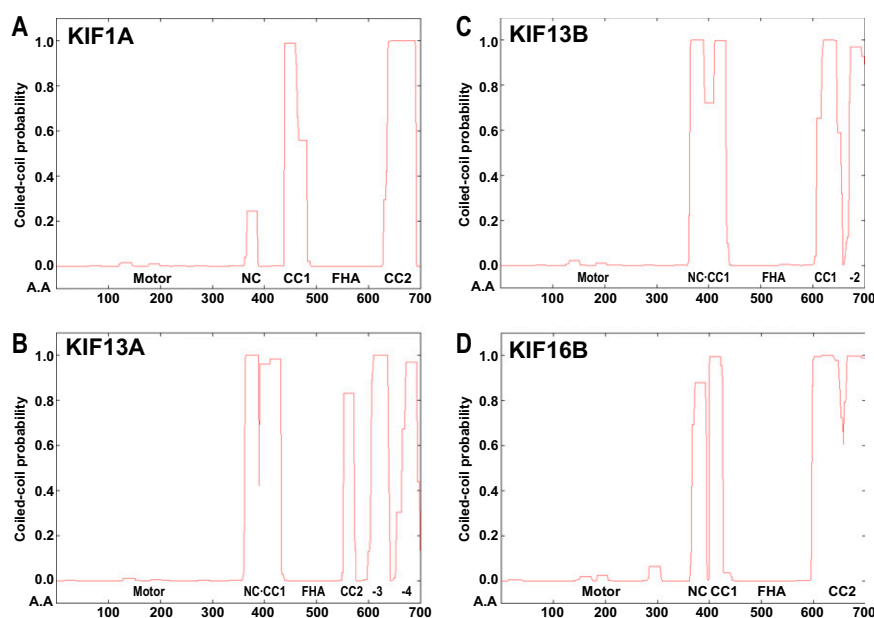


**Fig. S5.** Coiled-coil predictions for kinesin-3 motor proteins. (A–D) The probability of coiled-coil formation within the first 700 aa of the indicated kinesin-3 motor proteins was determined using the COILS program (1) (21-aa window). AA, amino acid; CC, coiled-coil; FHA, fork-head associated; NC, neck coil.

- Lupas A, Van Dyke M, Stock J (1991) Predicting coiled coils from protein sequences. *Science* 252(5009):1162–1164.







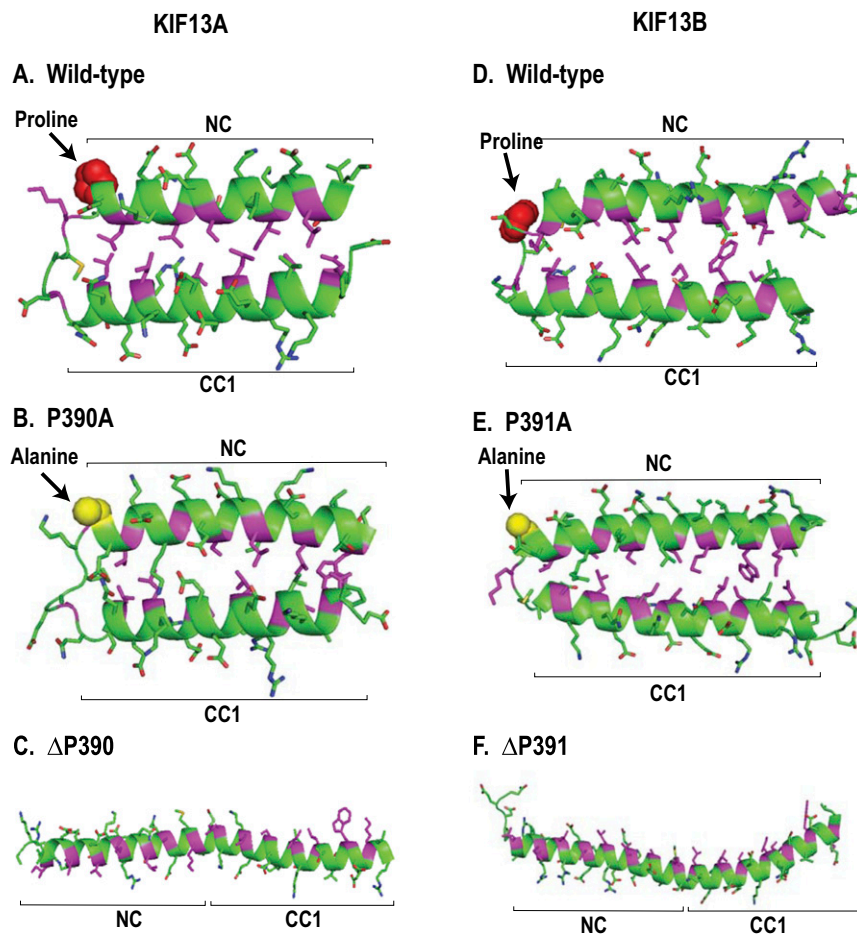


**Fig. S8.** Structural modeling of the NC–CC1 region of the KIF13 motors. The NC–CC1 amino acid sequences of KIF13A and KIF13B were subjected to computational protein structure prediction using I-TASSER (<http://zhanglab.ccmb.med.umich.edu/I-TASSER/>). For all sequences, only the predicted structures with the highest confidence score are shown. (*A* and *D*) For the wild-type protein sequences, the proline residues (red spheres) at the NC/CC1 junction cause a tight bend that allows the NC and CC1 sequences to interact in an antiparallel coiled-coil in the monomeric state. (*B* and *E*) Mutation of the proline residue to an alanine (yellow sphere) retains the tight bend at the NC/CC1 junction such that the antiparallel coiled-coil is preserved. (*C* and *F*) Deletion of the proline residue relieves the tight bend and results in the formation of a single long  $\alpha$ -helix that can homodimerize with another KIF13A or KIF13B polypeptide. The proline and alanine residues are shown in sphere representation, whereas the remaining residues are shown in ribbon representation. Magenta coloring indicates residues in the “a” and “d” positions of the heptad repeats.





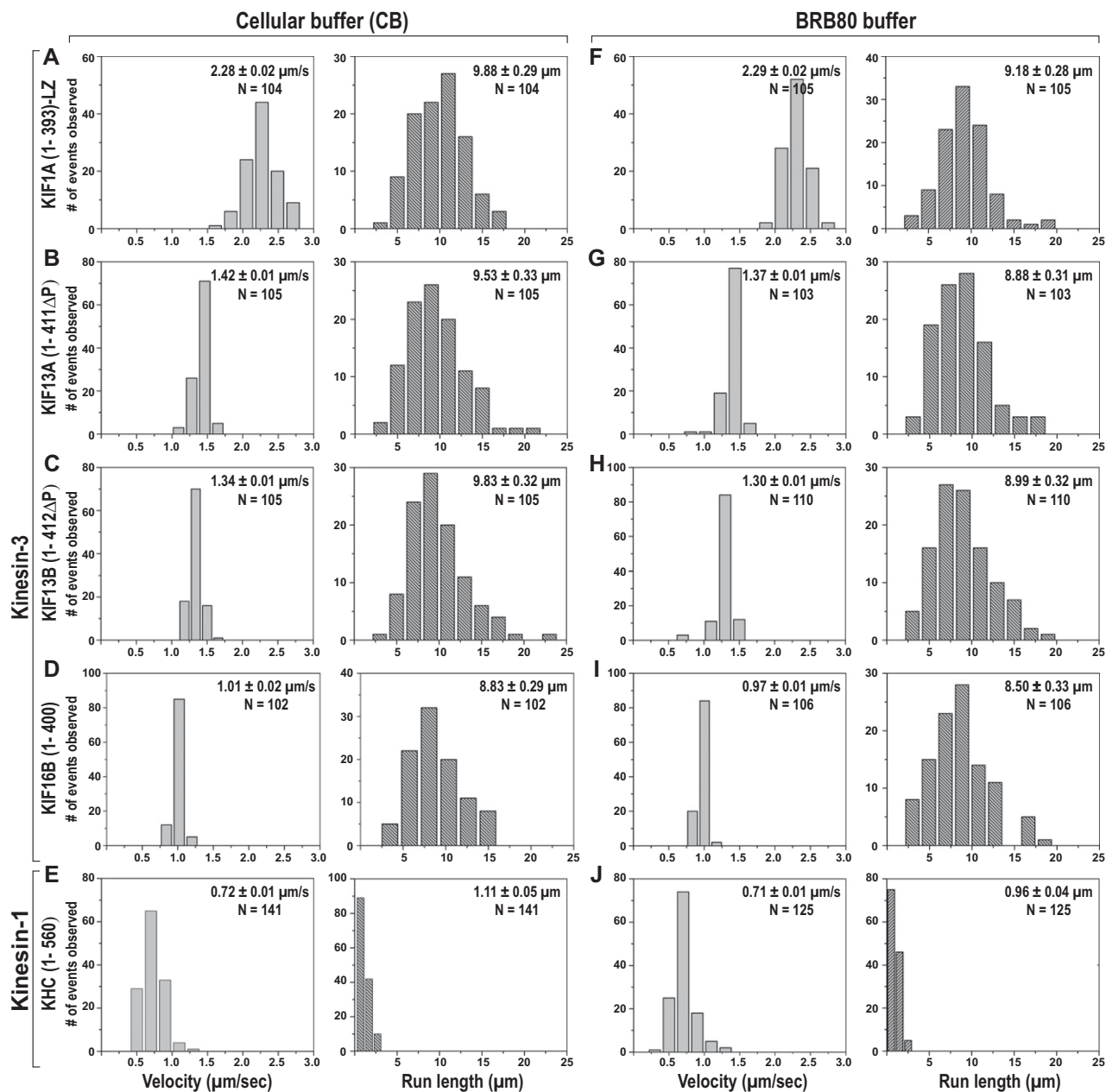


**Fig. S10.** Physiological ionic strength buffers do not affect the motility properties of kinesin-3 and kinesin-1 motors; 3xmCit-tagged motors in COS-7 cell lysates were added to polymerized microtubules in a flow chamber and observed by TIRF microscopy. Assays were carried out under physiological ionic strength conditions using (A–E) Cellular buffer (CB) meant to mimic intracellular conditions or (F–J) BRB80, a common high-ionic-strength motility buffer. Histograms of the velocities and run lengths were plotted for each population of motors. The peak represents the average velocity (Left) and run length (Right) of (A and F) KIF1A(1–393)-LZ, (B and G) KIF13A(1–411ΔP), (C and H) KIF13B(1–412ΔP), (D and I) KIF16B(1–400), and (E and J) KHC(1–560). Data are the averages from at least two independent experiments. The averages (mean ± SEM) and N values for each population are indicated in the top right corner of each graph.





**Table S2. Summary of single-molecule properties of active kinesin-3 motors**

Motor protein	Truncation/mutation	Oligomeric state	Velocity, $\mu\text{m/s}$ mean $\pm$ SEM	Run length, $\mu\text{m}$ mean $\pm$ SEM	No. of events observed
P12 buffer					
Kinesin-3 motors					
KIF1A	1-393	Dimer/monomer	$1.49 \pm 0.02$	$2.61 \pm 0.10$	155
KIF1A	1-393-LZ	Dimer	$2.45 \pm 0.02$	$9.80 \pm 0.14$	145
KIF13A	1-411 $\Delta$ P	Dimer	$1.41 \pm 0.01$	$10.71 \pm 0.22$	148
KIF13B	1-412 $\Delta$ P	Dimer	$1.31 \pm 0.01$	$10.14 \pm 0.23$	152
KIF16B	1-400	Dimer	$0.95 \pm 0.007$	$9.49 \pm 0.22$	149
Kinesin-1					
KHC	1-560	Dimer	$0.85 \pm 0.03$	$1.22 \pm 0.09$	191
Cellular buffer					
Kinesin-3 motors					
KIF1A	1-393-LZ	Dimer	$2.28 \pm 0.02$	$9.88 \pm 0.29$	104
KIF13A	1-411 $\Delta$ P	Dimer	$1.42 \pm 0.01$	$9.53 \pm 0.33$	105
KIF13B	1-412 $\Delta$ P	Dimer	$1.34 \pm 0.01$	$9.83 \pm 0.32$	105
KIF16B	1-400	Dimer	$1.01 \pm 0.02$	$8.83 \pm 0.29$	102
Kinesin-1					
KHC	1-560	Dimer	$0.72 \pm 0.01$	$1.11 \pm 0.05$	141
BRB80 buffer					
Kinesin-3 motors					
KIF1A	1-393-LZ	Dimer	$2.29 \pm 0.02$	$9.18 \pm 0.28$	105
KIF13A	1-411 $\Delta$ P	Dimer	$1.37 \pm 0.01$	$8.88 \pm 0.31$	103
KIF13B	1-412 $\Delta$ P	Dimer	$1.30 \pm 0.01$	$8.99 \pm 0.32$	110
KIF16B	1-400	Dimer	$0.97 \pm 0.01$	$8.50 \pm 0.33$	106
Kinesin-1					
KHC	1-560	Dimer	$0.71 \pm 0.01$	$0.96 \pm 0.04$	125
Full-length motors					
Kinesin-3 motors					
KIF1A	L478Q/M481Q	Dimer	$1.64 \pm 0.02$	$9.31 \pm 0.25$	172
KIF1A	V483N	Dimer	$1.80 \pm 0.03$	$9.00 \pm 0.23$	154
KIF13A	$\Delta$ P390	Dimer	$1.09 \pm 0.02$	$9.49 \pm 0.20$	161
KIF13B	$\Delta$ P391	Dimer	$1.08 \pm 0.01$	$9.25 \pm 0.19$	153
Kinesin-1					
KHC	1-560	Dimer	$0.81 \pm 0.03$	$1.04 \pm 0.05$	188